Micro/nano-structural evolution in spruce wood during soda pulping

Original article

Ahmed Wagih, Merima Hasani*, Stephen A. Hall and Hans Theliander

Micro/nano-structural evolution in spruce wood during soda pulping

https://doi.org/10.1515/hf-2020-0113
Received May 6, 2020; accepted December 1, 2020;
published online January 6, 2021

Abstract: Alkaline delignification of wood tissue is the core of the global pulping technology and the most prominent large-scale separation of the main wood components. This work aims at improved understanding of the interplay between the topochemistry of alkaline pulping and the associated morphological changes. Morphology and chemical structure of partially soda-delignified wood chips were studied combining X-ray tomography (XRT), X-ray diffraction analysis and compositional characterization (lignin and carbohydrate content). The XRT studies of wet samples (providing 3D structural information without interfering drying effects), allowed observation of the cell wall separation as an increasing amount of lignin was removed with the increasing pulping time. Comparison between the microstructure of the surface and the central parts of the treated chips showed a more delignified microstructure at the surface, which highlights the dependence of the delignification process on the mass transport (hydroxide ions and lignin fragments) through the wood tissue. The crystallite size of cellulose increased in the <200> crystal planes during the early stage of pulping while there was little effect on the <110> plane.

***Corresponding author: Merima Hasani,** Forest Products and Chemical Engineering, Chalmers University of Technology, SE-412 96, Gothenburg, Sweden; and Wallenberg Wood Science Center, Chalmers University of Technology, SE-41296 Gothenburg, Sweden, E-mail: merima.hasani@chalmers.se
Ahmed Wagih, Forest Products and Chemical Engineering, Chalmers University of Technology, SE-412 96 Gothenburg, Sweden; and Mechanical Design and Production Department, Faculty of Engineering, Zagazig University, P.O. Box 44519, Zagazig, Egypt. https://orcid.org/0000-0003-2782-6198
Stephen A. Hall, Division of Solid Mechanics, Lund University, Lund, Sweden; and Lund Institute of Advanced Neutron and X-ray Science, Lund, Sweden
Hans Theliander, Forest Products and Chemical Engineering, Chalmers University of Technology, SE-412 96 Gothenburg, Sweden; and Wallenberg Wood Science Center, Chalmers University of Technology, SE-41296 Gothenburg, Sweden

Keywords: delignification; microstructure; soda pulping; spruce wood; X-ray tomography.

1 Introduction

Climate change, and the associated necessity to reduce the use of fossil-based fuels, materials and chemicals, is one of the most urgent problems the world is currently facing. Therefore, during the last decades, there has been an increasing number of initiatives to develop new sustainable energy and material resources (Christopher 2013; De Bhowmick et al. 2017; Lew et al. 2012; Mattsson et al. 2017). Natural resources such as water, wind, solar energy and, to a certain extent, biomass are promising sources of clean and safe energy. Furthermore, the utilization of biomass via various biorefinery concepts provides a sustainable raw material basis for production of materials and chemicals. Wood is the most abundant biomass on land and is already one of our most important raw materials for the production of a large number of products used in our daily life, ranging from sawn timber (wood construction, furniture etc.) and fiber-based materials (paper, board, viscose) to chemicals (e.g. cellulose derivatives and lignosulfonates). Currently, the largest industrial use of wood is in the form of sawn timber and paper/board.

Kraft pulping is the most common process used to separate wood constituents and primarily recover cellulose fibers for paper, textile and cellulose derivative applications, while the main part of hemicelluloses and lignin (about 50% of the wood mass) are partly degraded, dissolved and, in a latter step, incinerated for energy needs of the process. A modern kraft pulp mill is, however, rather energy efficient and has a surplus of energy, which opens up an opportunity to extract some of dissolved components to be used as building blocks for production of various materials and chemicals (e.g. carbon fibers and furfural). This requires a better knowledge regarding different process steps in a pulp mill and how these influence the main product, the paper pulp. The most important operation in the paper pulp process is the pulping, where the partial fragmentation and dissolution of lignin and hemicelluloses

takes place and the individual fibers are liberated from the wood matrix (Gellerstedt 2009; Gierer 1980; Gustafson et al. 1983; Jansson and Brännvall 2014; Kwasniewski and Theliander 2001). It is, therefore, of no surprise that a vast number of publications elaborating on the main reaction pathways involved in this operation and the final fiber properties as functions of process conditions can be found in the literature (e.g. Brännvall 2009; Gomes et al. 2014; Singh et al. 2014). Numerous attempts to shed light on the topochemistry of pulping have involved investigations of the pulping chemicals diffusion paths in relation to anatomical features of wood (Wardrop and Davies 1961; Wardrop 1963), pulping studies on the isolated morphological motifs (Wood et al. 1972; Whiting and Goring, 1981), including UV microspectrophotometry (UMSP) studies (Kerr and Goring 1975; Procter and Goring 1967) and SEM EDAX investigations of the partially delignified samples (Saka et al. 1982). They pointed out a more rapid delignification of the secondary wall compared to the middle lamella along with the importance of the evolving cell wall porosity for the mass transport of the lignin fragments. However, comprehensive understanding of the interplay between the topochemistry and the morphological changes during pulping calls for additional work (e.g. investigations of the different substeps in relation to solubility and mass transport of the wood components), not the least imaging efforts that would provide the necessary morphological dimension.

Understanding of the correlation between the chemical and morphological changes during pulping is a prerequisite for an efficient process-structure-property control and is, as such, of increasing importance for the pulping industry that is facing a growing need for material efficiency and diversification. Elucidating the sequence of morphological and micro-/nano-structural changes during delignification process is a key for a better understanding of how the pulping conditions influence the properties of the produced cellulose pulp.

X-ray tomography (XRT) is an established, non-destructive technique for qualitative and quantitative 3D structural evaluations of materials in many fields, such as damage inspection (Bull et al. 2013, 2014; Wagih et al. 2019) and structural evolution (Ji et al. 2014; Taiwo et al. 2017; Van den Bulcke et al. 2013). The technique involves acquiring a set of 2D-projections at different angles during the rotation of the object around a pre-defined axis and reconstructing a 3D image of the object microstructure (Webb 1990). Thus, XRT has the advantage, over conventional structural inspection methods such as Scanning Electron Microscopy (SEM) and Transmission Electron Microscopy (TEM), of providing information in 3D volumes. Applied to wood, the XRT has been demonstrated to be a powerful imaging technique allowing both qualitative and quantitative anatomic analysis (Van den Bulke et al. 2008), and material development investigations (Van den Bulke et al. 2009). Synchrotron XRT was employed by Hass et al. (2010) for more detailed anatomical studies focusing on vessel size. Structural changes in wood accompanying drying (Derome et al. 2011; Lazarescu et al. 2010) and different types of processing – whether aiming at separation of wood components or modification of wood tissues for material applications – have also been studied by XRT (Faessel et al. 2005; Muzamal et al. 2016; Walther et al. 2009; Walther and Thoemen 2009). However, all the aforementioned studies have been performed on dry or purposely dried samples. There is a lack of structural analysis of wood during chemical modifications (without drying) even by using electron microscopy (due to the difficulties of keeping samples wet during inspection because of nitrogen gas and vacuum application). Additionally, due to the small thickness of samples required for TEM (about 100 μm), surface tension of the wood samples is an issue that makes such an inspection extremely difficult.

This study investigates the microstructural evolution in spruce wood during a simplified version of kraft pulping relying only on the action of hydroxide ions – so-called soda pulping. XRT is used to study wet and dried material and the observed structural changes are correlated with the chemical analysis of the samples and the nanostructural changes investigated by X-ray diffraction. A batch approach was applied in the pulping experiment and the residence time was varied. Both wet and dried samples were characterized to highlight the influence of drying on the structural changes. Cell wall thickness of the wet and dried samples and cell shape and size were analysed from the XRT images. Based on the obtained results, a detailed sequence of microstructural changes during soda pulping could be presented.

2 Materials and methods

2.1 Sample preparation and soda pulping experiment

The raw material used in this study was spruce wood. A piece of wood (dimensions: $140 \times 10 \times 10$ mm^3) was cut from the sapwood of the tree with major dimension in the longitudinal fiber direction. This large piece was divided with a band saw into small samples with dimensions $20 \times 5 \times 5$ mm^3 as shown in Figure 1. The obtained samples were divided into six batches. Each batch, containing four samples, was cooked for predefined time: 30, 60, 90, 120, 150 and 180 min. A batch of four samples was kept as reference samples without any treatment.

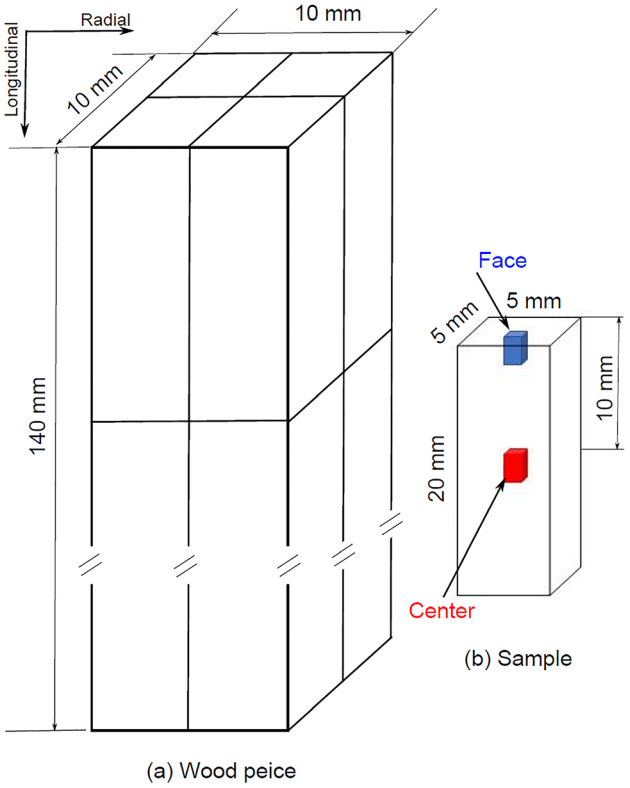

Figure 1: Schematic drawing of the sample cut showing (a) the dimensions and fiber directions and (b) the size of the sample with the regions of XRT inspections.

A soda pulping of the samples was performed in autoclaves (1.5 L) placed in a rotating rig in a temperature-controlled polyethylene glycol bath. A solid to liquor ratio of 1:100 was used to achieve a near constant bulk concentration. The cooking liquor was prepared by adding 1066 g of DI water to 34 g of pellets NaOH 98% (sodium hydroxide) resulting in a 3 wt. % NaOH(aq).

Six autoclaves were charged with wood samples and the cooking liquor (deaerated under vacuum for 5 min and pressurized to five bars with nitrogen gas for 5 min to ensure good impregnation and an oxygen free environment), then depressurized and placed in the heating vessel at a temperature of 170 °C. The complete temperature change inside the autoclaves has been measured in earlier studies (Wigell et al. 2007). When the predefined time was reached, each of the autoclaves was cooled in a water bath and the cooking charge was filtered using a Büchner funnel with a polypropene mesh. The filtered samples were then washed with 2 L of deionised water and kept in deionised water for two days before being extensively washed again – the procedure was assumed to remove all dissolved material. One sample of each batch was oven dried at 40 °C for 72 h.

2.2 Klason lignin and carbohydrate analysis

For chemical analysis, the wood samples were milled in a Wiley-type mill, oven-dried and subjected to complete acid hydrolysis using 72% sulfuric acid. The residual solid material was considered to be Klason lignin, the amount of which was determined gravimetrically. The filtrate from the hydrolysis was used to determine the contents of acid soluble lignin (ASL) and carbohydrates (Theander and Westerlund 1986).

The carbohydrate composition was determined as the amount of monomeric sugars by using high-performance anion exchange chromatography (HPAEC) with a Dionex ICS-5000 equipped with a CarboPacTM PA1 column and an electrochemical detector; NaOH and NaOH + NaAc were used as eluents. The Chromeleon 7, Chromatography Data System, Version 7.1.0.898 software was used for the analysis. The amounts detected were corrected to the hydrolysis yield. The hydrolysis yield was calculated from experimental data, established by performing acid hydrolysis on pure monosugar standards (Wojtasz-Mucha et al. 2019), as the ratio of the amount detected to the mass of the sample used: for arabinose, 93.1 ± 1.9%, galactose, 92.9 ± 1.7%, glucose, 91.8 ± 2.0%, xylose, 78.6 ± 1.6%, and mannose, 90.2 ± 0.6%.

2.3 Microcomputed X-ray tomography and X-ray diffraction

The microstructure of the pulped samples was investigated using XRT with a Zeiss XRadia XRM520 at the 4D Imaging Lab of Lund University. Prior to imaging, to accurately observe cell walls whose size can be as small as a few hundred nm (Muzamal et al. 2016), we set a voxel pitch of 0.55 µm. This required us to trim down the samples to smaller squared cross-sections of about 2×2 mm^2. The samples were covered with commercial thin paraffin-based film (parafilm®) to avoid drying during the XRT measurements. The X-ray source settings were 80 kV and 7 W with an exposure time of 2.75 s for each projection. These raw projections were reconstructed using Zeiss tomographic reconstructor software to yield image volumes with $0.55 \times 0.55 \times 0.55$ µm^3 voxel size and a field of view of about 550 µm wide and high, i.e., the image volumes covered internal region of the samples, thus avoiding any surface disturbance due to cutting. The image volumes were binarized using the ImageJ software to easily quantify the cell wall thickness (width of the bright phase) and tracheid size (width of the dark phase). These were then measured using the measuring tool in ImageJ. Some of the samples were inspected twice: at the upper face and at the sample center, as shown in Figure 1.

The nanostructure of the pulped samples was inspected using a X-ray diffractometer (PANalytical X'Pert Pro with a Cu tube (λ = 1.5404 Å) at Chalmers University of Technology). Prior to inspections, dried samples were ground to fine particles, ~500 µm, using mechanical grinder for 2 min. Powder samples were placed on a low-background quartz holder and subjected to radiation at 25 mA and 35 kV. A step size of 0.1° and 5 s exposure were used for measuring the scattering angle 2-θ in the range 5–40°. Three powder samples were tested for each configuration. The crystallite size was estimated using the Scherrer equation (Wernersson et al. 2013):

$$D = \frac{0.9\lambda}{B\cos\theta} \quad (1)$$

Where D, B, λ and θ are crystallite size (nm), full width at half maximum (FWHM), the wavelength (λ = 0.15406 nm) and peak position, respectively.

The FWHM is measured by identifying the height of the maximum value of a peak, then constructing a horizontal line at the half of this height intersecting the peak in two points, i.e. two different angles. The difference between these two angles corresponds to the FWHM.

3 Results and discussion

3.1 Compositional changes during pulping

Table 1 shows the polymer content, (galacto)glucomannan (GGM), xylan, cellulose and lignin, in the starting material and the pulped samples as a function of pulping time. The undetected material likely contains acid soluble lignin structures (not quantified in this study), carbohydrate degradation products and extractives.

The composition of the starting material – the comparably low cellulose content, along with the high lignin content – indicates that the samples originated from a compression wood (Nanayakkara 2009; Timell 1986). The micrographs of the transverse cross section of the analyzed samples are in line with these indications showing rounded tracheids with intercellular space, typical of compression (Figure 2). Compression wood is, namely, characterized by a higher lignin content with a more condensed structure, along with reduced content of cellulose, xylan and mannan relative to normal wood. Compression wood cells are also shorter, thicker and rounder and are unique in containing β-1,4-galactan (Mast et al. 2009; Morohoshi and Sakakibara 1971a,b; Nanayakkara et al. 2009; Timell 1986). Delignification of compression wood has been reported to yield pulps with coarser fibers and a higher amount residual lignin containing more condensed motifs and galactan residues, the latter suggested to originate from the outer layers of the fiber wall (Hortling et al. 2001). Delignification studies with alkaline nitrobenzene oxidation have reported a slower leveling off of the delignification for compression wood leading though eventually to approximately same level of residual lignin as in normal wood (Yoshinaga et al. 2014).

As expected, the majority of GGM was removed during the early stage of pulping (initial 30 min), mainly due to the high rate of the peeling reaction of GGM compared to the other carbohydrates. During this initial phase the GGM content was reduced by approximately 45% reaching a largely stable residual content after 60 min. Similar behavior of GGM was also observed during soda delignification of softwood meal under comparable conditions (3% NaOH[aq], 168 °C): rather stable residual content after a rapid initial removal (Wigell et al. 2007). The decrement in the xylan content was rather modest through the process for all the considered samples, which is also in line with the previous findings. The lignin content decreased with increasing pulping time (the removal rate is higher) at the early stage until 90 min, showing no significant changes during further pulping. Not surprisingly, considering the size and character of the studied samples (sticks of lignin rich reaction wood), delignification of softwood meal under comparable conditions (3% NaOH[aq], 168 °C) was found to be considerably faster removing approximately 50% of lignin after ca. 60 min pulping (Wigell et al. 2007). The relative cellulose content in the sample increased with increasing pulping time up to 150 min, due to the removal of the other polymers (mainly GGM and lignin). Further pulping led to a decrease of cellulose content, due to continued reactions (peeling and alkaline hydrolysis).

Table 1: Polymer content (%) of the dried samples as a function of pulping time.

Pulping time (min)	(Galacto)glucomannan (GGM)	Xylose	Klason Lignin	Cellulose
0	13.4	4.9	30.7	33.6
30	7.4	5.8	24.9	45.5
60	6.5	4.9	22.9	56.9
90	6.8	4.2	19.8	64.4
120	6.0	4.1	18.5	69.6
150	6.9	3.7	19.4	75.8
180	5.0	4.5	17.3	71.7

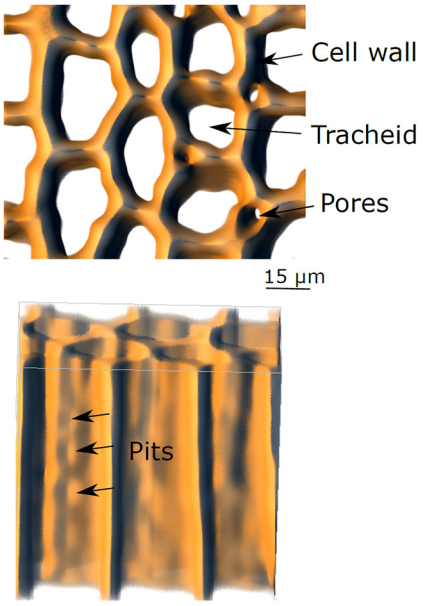

Figure 2: Internal microstructure of spruce wood in transverse and tangential cross section.

3.2 Microstructural evolution

The tangential and transverse section of the XRT images of the untreated wood are shown in Figure 2, where the structure of the tracheids and the pits inside the cell walls are visible. The tracheids are intact without any evidence of

micro cracks or decohesion. The pits that can be observed are so-called bordered pits and have a total width of approximately 3 µm, including the border. These openings have a membrane of less than 1 µm thickness (Muzamal et al. 2016; Skaar 1988), which cannot be observed in the current study as they are below the resolution of the images. These pits are the only passages between tracheids and, therefore, control the transport of liquors and ions between them. The cross-section shapes of the tracheids (some of them elongated and elliptical) are also captured (see Supplementary Figure S1). The presence of elliptical tracheids, and the small pores between them (transverse cross section), is typical of reaction wood and is in accordance with previous experimental observations on spruce wood (Muzamal et al. 2016; Trtik et al. 2007; Van den Bulcke et al. 2013).

Figure 3 shows the variation of sample weight (wet and dry) as a function of pulping time. Four stages can be defined based on the sample weight evolution. Stage I ranges from the start of the pulping until 30 min, during which the weight of the wet samples increased to around four times that of the untreated wood, which is interpreted as being due to filling of the lumen, as well as the absorption and saturation of cell walls with cooking liquor (see Figure 4b). During pulping, the cooking chemicals (in this case the hydroxide ions) need to be transported (diffusive mass transport) in the wood tissue to the reaction site in the cell wall and/or mid-lamella. In softwood, the dominating path for this transport is via lumen of the tracheids. Pits provide transport between the adjacent cells organized in rows with overlapping ends (mass transport in the longitudinal direction). In the radial and transversal direction, the transport paths are via rays and pits between the cells. Muzamal et al. (2016) visualized pits by high-resolution XRT, without capturing their membranes due to the resolution limit. Resin canals contribute also with additional transportation path. As hemicelluloses and lignin are gradually removed (see Table 1) during pulping, voids can be seen being formed in the cell walls and in the upper surface of the wood samples (see Figure 4b); such cavities provide another important transportation path for the cooking liquor. The mentioned transport paths enable saturation of the cell walls and, as seen in Table 2, results in an increase in the wall thickness and reduction of the inner diameter (due to the swelling of the cell wall) (Figure 4b). Similar results have been reported by Van den Bulcke et al. (2013).

During stage I, the dominating process is the removal of hemicelluloses, as shown in Table 1. This process enhances the transport of hydroxide ions to the middle lamella by diffusion through the formed voids. Lignin is gradually removed as well (see Table 1), further facilitating diffusion of cooking liquor to the middle lamella that

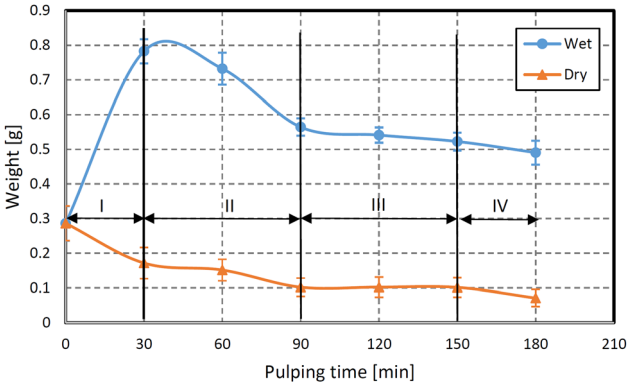

Figure 3: Weight evolution of spruce wood during pulping process.

contains structurally different lignin (Chiang et al. 1989; Whiting and Goring 1982). This saturation of the wood tissue with the cooking liquor (lumen, pits and the

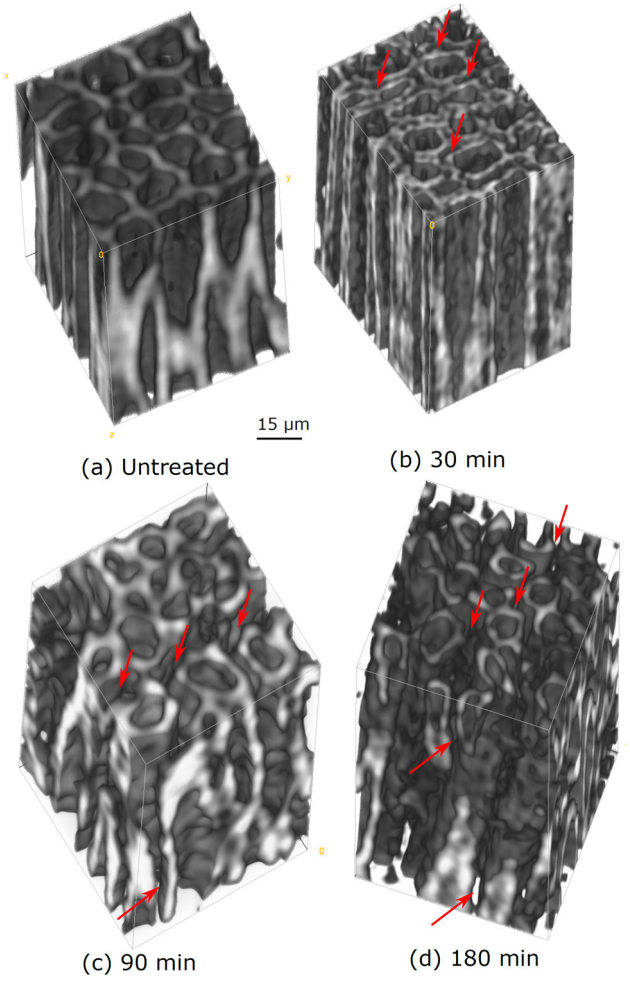

Figure 4: µCT micrographs of wet samples at different pulping times. The micrographs are captured at the transverse cross sections of the samples surface. The red arrows refer to the cracks and separation of cell walls.

Table 2: Variation of wall thickness with pulping time.

Pulping time (min)	Wall thickness (µm)	
	Wet	Dry
0	3.75 ± 0.05	3.75 ± 0.05
30	4.67 ± 0.12	2.73 ± 0.16
90	4.01 ± 0.12	2.09 ± 0.10
180	3.92 ± 0.14	–

emerging voids due to removal of hemicellulose and lignin), is also expressed in the macrostructure of the samples. An increase in the sample volume and erosion of the initial edges (possibly indicative of changes in individual tracheids) are evident in Figure 5, which shows photos of the untreated and pulped samples. Indeed, changes in the individual tracheids during this stage can be seen in Figure 4b. At the same time, the data on the dried samples shows a reduction of the dry weight during stage I, which is in line with the removal of lignin and hemicelluloses (Table 1). Accordingly, the cell wall thickness of the dried samples reduced to 2.73 µm after 30 min pulping compared to a thickness of 3.75 µm for the untreated samples; corresponding to a thickness reduction by one third. As shown in Figure 6a, separation of cell walls initiated during this stage at the external surface extended in the lateral direction of cell walls; this is likely due to the removal of the lignin from the middle lamella and can also be seen in the images of the wet samples in Figure 4b. Thus, two main processes seem to control the structural changes during stage I (surface sample): (i) saturation of cell walls with the cooking liquor along with removal of hemicelluloses and (ii) partial removal of lignin, affecting also middle lamella.

Stage II continued to approximately 90 min of pulping and during this time the weight of the wet samples reduced, likely related to the continued removal of the polymer residues from the liquor-saturated cell walls, which is the dominating process at this point. During this

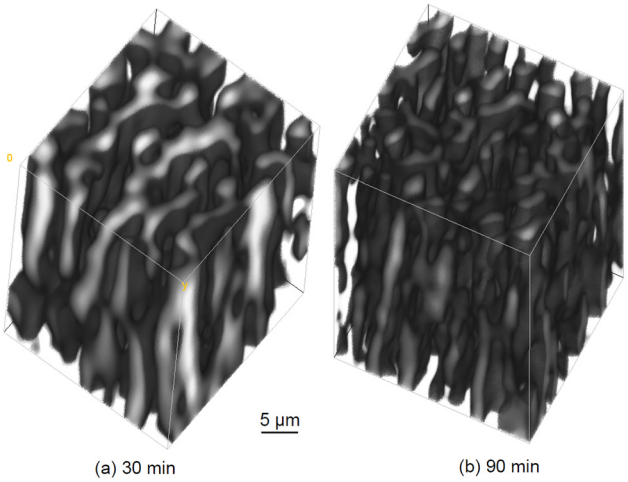

Figure 6: µCT micrographs of dry samples surface at different pulping time.

stage, due to the high removal of lignin, the microstructure of the sample pulped for 90 min showed a clear separation of cell walls, Figure 4c. The tracheids at this stage appeared to have untied from the initial tissue matrix adopting a drastically changed (almost circular) shape (Figure 5). Due to removal of lignin and hemicelluloses, the weight of dried samples reduced during this stage (see Figure 3) from 0.29 g, after 30 min pulping, to 0.10 g after 90 min. While the wall thickness reduces from 2.73 µm at the beginning of the stage to 2.09 µm at the end, corresponding to a 23.2% reduction. The cell wall thickness of the corresponding wet samples reduced from 4.67 to 4.01 µm. By the end of this stage, the separation of the cells initiated during stage I appears to be completed. Furthermore, microcracks could be observed inside the cell walls on the XRT image in Figure 6b.

Stage III corresponds to the continued pulping until 150 min, during which the samples weight only changed slightly (see Figure 3), with the microstructure more or less unchanged (see Figure 4). Interestingly a further extension of the pulping time to 180 min, led to a slight reduction in the wet and dry sample weight (see Figure 3), which could

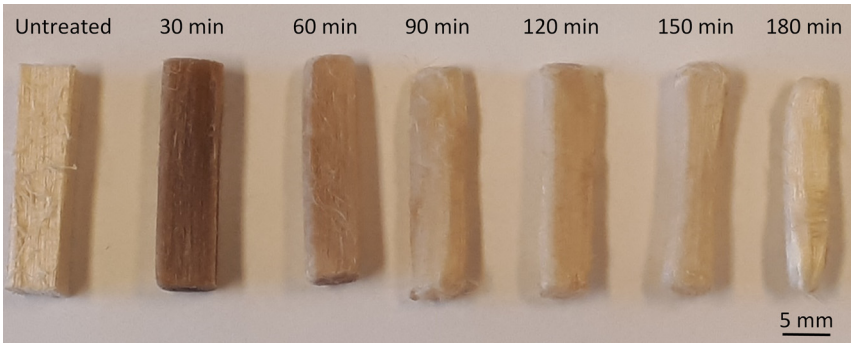

Figure 5: Photos of wet samples before pulping and after different pulping time.

be defined as an additional stage, IV. During this stage (IV) the microstructure of the sample (Figure 4d) remained quite similar to that observed in the samples pulped for just 90 min. The cell wall thickness slightly reduced (from 4.01 to 3.92 µm for samples pulped at 90 and 180 min, respectively). The slight reduction of the weight and cell wall thickness is attributed to the reduction of cellulose content (see Table 1) due to the degrading cellulose reactions (peeling and alkaline hydrolysis) with the excess cooking liquor mediating dissolution. Still the cell walls of the sample pulped for 180 min were thicker than those of the untreated sample, probably due to the saturation of the cell walls with water.

3.3 Local variations in microstructural and compositional changes

Figure 7 shows the XRT images of the microstructure for the regions near the surface and center of the samples pulped for 30 min and 90 min. The microstructure near the sample surface shows an initial cell wall separation between almost all the cells after only 30 min pulping (see Figure 7a). The separation between the walls can be seen to extend in some cells in the longitudinal direction, as marked by the red ellipse in in Figure 7a. However, Figure 7b shows the microstructure at the center of the same sample where the tissue appears to be completely intact, except for a small separation between two of the cell walls. This separation might be due to the presence of pits between these walls, which could have facilitated transport of the hydroxide ions between tracheids to enable lignin removal at the middle lamella. The thickness of the cell walls at this initial stage of pulping was almost the same in the images from the surface and the center of the sample, which highlights that, at this time, the whole sample was impregnated with the cooking liquor. However, no obvious morphological changes could be observed in the image of the center of the sample, for which there are likely two main reasons. Firstly, the hydroxide ions entering the wood chip would have reacted as soon as they reached a reactive wood component, which would have occurred close to the surface of the wood chip. Secondly, the ions hade to be transported a long distance by diffusion before they reached the center of the wood chip. Therefore, both chemical reactions and mass transport of ions should be considered as the key parameters governing the chemical pulping at this stage. The microstructure of the sample's surface pulped at 90 min showed complete separation of cell walls in images from near the surface (see Figure 7c). The separation could also be seen to extend to the center of the sample (see Figure 7d) so the cells are more or less completely separated throughout the sample, which indicates that the delignification process was largely complete by the end of stage II (90 min of pulping) at the used conditions. As the soda pulping chemistry in general does not allow cleavage of phenolic β-O-4′ bonds in lignin, while relying on a rather slow cleavage of non-phenolic β-O-4′ bonds, a considerable amount of residual lignin (too large to be solubilized and transported out) remains in the wood tissue at this point (Fengel and Wegener 1984; Walker 2006; Zhao et al. 2019).

It is obvious that the structure of spruce wood dramatically changes during the soda pulping process as shown in Figures 4, 5, and 7. In the initial phase the temperature increases, but remains relatively low, so the reaction rates are also low and the ions can be transported via lumen and pits into the cell walls. In the beginning of this low-temperature stage it is mainly glucomannans that react (the peeling reaction), but this occurs rather slowly at temperatures below 70 °C. Thus, in the very beginning it is mostly mass transport of alkali that takes place resulting in neutralization of acid groups, an increased pH in the wood and, as a consequence, swelling of the cell walls (see Table 2). As the temperature increases the peeling reaction rate increases, including reactions of xylan and cellulose, as well as various lignin reaction consuming the hydroxide

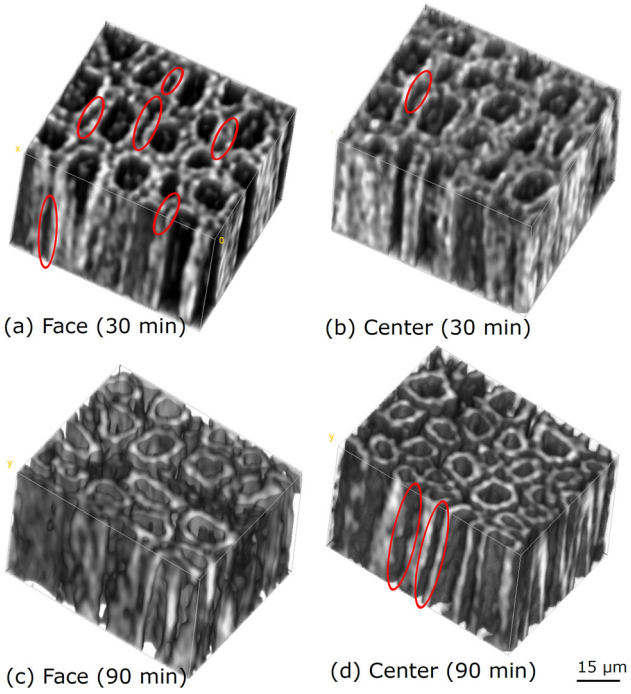

Figure 7: µCT micrographs of wet samples at their faces and centers pulped for 30 and 90 min.

ions inside the wood chip (see Table 1). Since the reaction rate increases much faster than the diffusive mass transport when the temperature is increased, there will be a point at relatively low temperature where more ions are consumed than what can be transported into all parts of the wood chip. At this point the majority of the hydroxide ions entering the wood chip are consumed close to the sample surface causing a detectable separation of the cell walls (see Figure 7a). The exact temperature when this occurred is not yet known and will vary with e.g. wood structure, chip size, chemical composition, but it is expected to be somewhere between 70 and 100 °C. When the hemicelluloses and lignin in this region react, they dissolve and diffuse out from the cell wall towards the surface of the wood chip. As more wood constituents are dissolved, less hydroxide ions are consumed close to the surface. This implies that the hydroxide ions entering the wood chips were transported deeper into the chips and started to react with the wood constituents. During this stage, the reduction rates of the dried sample weight and cell wall thickness are lower since the mass transport of hydroxide ions in the wood tissue to the reaction sites is relatively slow and the extractable hemicelluloses, which could contribute to further decrement of the dry weight, are already heavily depleted during the previous stage. In the stage III, the dry weight, polymer content and the cell wall thickness are stable (see Figure 3 and Tables 1, 2). On the other hand, development and extension of cracks inside the cell walls and the cell wall separation are visible, being the most prominent observed processes in this stage (see Figure 4c). Further pulping of the samples leads to a reduction of the cellulose content due to cellulose reactions with the cooking chemicals.

3.4 Nanostructure evolution

Figure 8 shows XRD patterns of the untreated sample and the pulped samples with the diffraction peaks labeled to indicate their crystal lattice assignments. Only two crystal lattice planes are defined in the figure for the simplicity of the analysis, the <110> and the <200>.

In the case of the <200> plane, peak broadening was observed with increasing pulping time up to 60 min, resulting in a decreased full width at half maximum (FWHM). Consequently, the crystallite size at this plane was inferred to have increased with increasing pulping time up to 60 min, reaching 3.38 nm compared to 1.89 nm for the raw material, as shown in Figure 9. The analysis of the <100> plane was complicated by the less well-defined peak shape. In fact, the literature reports on another minor

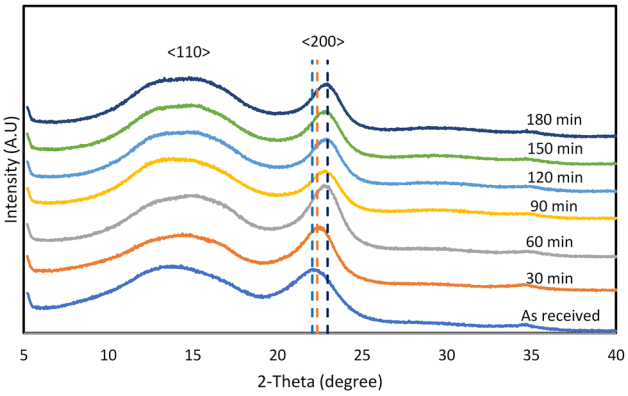

Figure 8: XRD patterns of as received and pulped samples at different times. The dash lines in the figure represents to the position of the <200> peak with corresponding color at different pulping time.

lattice plane located just after the <110> plane (Evstigneyev and Shashilov 1995; Lee et al. 2015; Park et al. 2010; Teeäär et al. 1987), which probably could give rise to the broad (double) peak. The average peak width and position did not show any significant discernable differences between the samples from different pulping times. The average crystallite size in this plane could be estimated to 1.18 nm, and it was relatively constant for all the pulped samples, as shown in Figure 9.

The increase of crystallite size, seen in the <200> reflection, could be attributed to the high temperature applied during pulping, 170 °C, which could have facilitated grain growth and recrystallization (Fan et al. 1980). Another reason for the crystallite size increase was the removal of lignin and hemicelluloses, allowing the lateral coalescence of cellulose crystallites and leading to the, commonly observed, increase in lateral fibril aggregate dimensions (Hult et al. 2001). During the early stage of

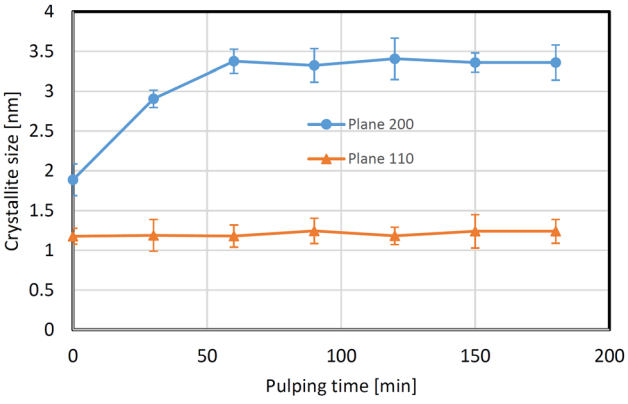

Figure 9: Variation of crystallite size with pulping time computed using Equation (1).

pulping (up to 60 min), the hemicelluloses and lignin removal rate were high (see Table 1), facilitating possibly an accelerated growth of cellulose crystallites. This also probably led to a slight increase in the 2-Theta angle of the <200> peak. After 60 min pulping, removal rate of the hemicelluloses was significantly slower (see Table 1) and the pulping process appeared to have no further influence on the <200> peak position.

4 Conclusions

The structural changes in wood during soda pulping have been studied using standard approaches combined with high-resolution X-ray micro-tomography and X-ray diffraction. Four stages could be identified in the pulping process. During the stage I (initial 30 min, approximately), the cooking liquor passes through the lumen and pits of the tracheids and saturates the inner surface of the cell walls, which results in an initial removal of hemicelluloses and lignin from the secondary wall. In this stage, the weight of the wet samples was around three times that of the unprocessed wood, due to the saturation of cell walls with the cooking liquor, while the dry weight was reduced, indicating an initial removal of lignin and hemicelluloses. The X-ray diffraction data for the <200> reflection of the cellulose indicated an increase in the cellulose crystallite size, also likely due the removal of lignin and hemicelluloses. After this stage (during the additional 60 min pulping), due to the continued removal of hemicelluloses and lignin from the secondary wall, the results suggest improved diffusion of the hydroxide ions through the cell walls resulting in a more pronounced lignin extraction from the cell walls and the middle lamella, which, thus, initiated cell wall separation. After 90 min pulping (stage III), the cell walls were visibly separated from each other due to the delignification of the middle lamella, whilst the microstructure, crystallite size, polymer content and wall thickness seem to remain largely unchanged during continued pulping until 150 min (stage IV). Further pulping led to reduction of the cellulose content related to cellulose reactions with the excess cooking chemicals.

The microstructure of the outer surface of the pulped samples was different from the sample core, highlighting that the delignification process occured in a successive manner, as the hydroxide ions passed through a complicated path until reaching the lignin in the middle lamella. Therefore, a homogenous microstructure of the pulped samples cannot be achieved at the start of the operation, and some time is needed to remove hemicellulose and lignin from the secondary wall, which then facilitates the transport of hydroxide ions to the middle lamella in the core. The mass transport of lignin and hemicelluloses is crucial during the soda pulping process. At the early stage of pulping, the transport of alkali to the secondary cell walls is dominant along with the mass transport of the depolymerized hemicelluloses and parts of lignin. While at late stages, the mass transport of lignin out of the cell walls becomes the main determinant for the morphology and microstructure.

Acknowledgments: We acknowledge Ms. Ximena Rozo Sevilla and Joanna Wojtasz-Mucha for their help in performing soda pulping experiment and chemical analysis.
Author contributions: All the authors have accepted responsibility for the entire content of this submitted manuscript and approved submission.
Research funding: The authors would like to acknowledge the ForMax pre-project initiative financed by the Swedish Government and the "FORMAX-portal – access to advanced X-ray methods for forest industry" (VR project number: 2018-06469).
Conflict of interest statement: The authors declare no conflicts of interest regarding this article.

References

Brännvall, E. (2009). Pulping technology. In: Ek, M., Gellerstedt, G., and Henriksson, G. (Eds.), *Pulp and paper chemistry and technology*. Berlin: Walter de Gruyter, pp. 121–148.

Bull, D.J., Helfen, L., Sinclair, I., Spearing, S.M., and Baumbach, T. (2013). A comparison of multi-scale 3D X-ray tomographic inspection techniques for assessing carbon fibre composite impact damage. Compos. Sci. Technol. 75: 55–61.

Bull, D.J., Spearing, S.M., and Sinclair, I. (2014). Observations of damage development from compression-after-impact experiments using ex situ micro-focus computed tomography. Compos. Sci. Technol. 97: 106–114.

Chiang, V.L., Stokke, D.D., and Funaoka, M. (1989). Lignin fragmentation and condensation reactions in middle lamella and secondary wall regions during kraft pulping of Douglas fir. J. Wood Chem. Technol. 9: 61–83.

Christopher, L.P. (2013). Integrated forest biorefineries: current state and development potential integrated forest. In: Christopher, L.P. (Ed.), *Biorefineries: challenges and opportunities*. Cambridge: RSC Green Chemistry Series, Royal Society of Chemistry, pp. 1–66.

De Bhowmick, G., Sarmah, A., and Sen, R. (2017). Lignocellulosic biorefinery as a model for sustainable development of biofuels and value added products. Bioresour. Technol. 247: 1144–1154.

Derome, D., Griffa, M., Koebel, M., and Carmeliet, J. (2011). Hysteretic swelling of wood at cellular scale probed by phase-contrast X-ray tomography. J. Struct. Biol. 173: 180–190.

Evstigneyev, E., and Shashilov, A. (1995). Cellulose recrystallization in the alkaline pulping of wood. In: Kennedy, J.F., Phillips, G.O., Williams, P.A., and Piculell, J.L. (Eds.), *Cellulose and cellulose derivatives*. Woodhead Publishing, Cambridge, UK, pp. 517–522.

Faessel, M., Delisée, C., Bos, F., and Castéra, P. (2005). 3D modelling of random cellulosic fibrous networks based on X-ray tomography and image analysis. Compos. Sci. Technol. 65: 1931–1940.

Fan, L.T., Lee, Y.H., and Beardmore, D.H. (1980). Mechanism of the enzymatic hydrolysis of cellulose: effects of major structural features of cellulose on enzymatic hydrolysis. Biotechnol. Bioeng. 22: 177–199.

Fengel, D. and Wegener, G. (1984). Alkaline pulping. In: Fengel, D. and Wegener, G. (Eds.), *Wood: chemistry, ultrastructure, reactions*. Berlin: Walter De Gruyter & Co, pp. 304–307.

Gellerstedt, G. (2009). Chemistry and chemical pulping. In: Ek, M, Gellerstedt, G., and Henriksson, G. (Eds.), *Pulp and paper chemistry and technology – pulping chemistry and technology*, Vol. 2. Berlin: De Gruyter, pp. 92–119.

Gierer, J. (1980). Chemical aspects of kraft pulping. Wood Sci. Technol. 14: 241–266.

Gustafson, R.R., Sleicher, C.A., McKean, W.T., and Finlayson, B.A. (1983). Theoretical model of the kraft pulping process. Ind. Eng. Chem. Process Des. Dev. 22: 87–96.

Gomes, F., Santos, F., Colodette, J., Demuner, I., and Batalha, L. (2014). Literature review on biorefinery processes integrated to the pulp industry. Nat. Resour. J. 5: 419–432.

Hass, P., Wittel, F.K., McDonald, S.A., Marone, F., Stampanoni, M., Herrmann, H.J., and Niemz, P. (2010). Pore space analysis of beech wood: the vessel network. Holzforschung 64: 639–644.

Hortling, B., Tamminen, T., and Pekkala, O. (2001). Effects of delignification on residual lignin-carbohydrate complexes in normal pine wood and pine wood enriched in compression wood. 1. Kraft pulping. Nord. Pulp Paper Res. J. 16: 219–224.

Hult, E.L., Larsson, P.T., and Iversen, T. (2001). Cellulose fibril aggregation — an inherent property of kraft pulps. Polymer 42: 3309–3314.

Jansson, Z.L. and Brännvall, E. (2014). Effect of kraft cooking conditions on the chemical composition of the surface and bulk of spruce fibers. J. Wood Chem. Technol. 34: 291–300.

Ji, Y., Hall, S.A., Baud, P., and Wong, T.F. (2014). Characterization of pore structure and strain localization in Majella limestone by X-ray computed tomography and digital image correlation. Geophys. J. Int. 200: 701–719.

Kerr, A.J. and Goring, D. (1975). The role of hemicelluloses in the delignification of wood. Can. J. Chem. 53: 952–959.

Kwasniewski, M. and Theliander, H. (2001). *Combined effect of heat transport and chemical kinetics on the delignification rate in wood chips*. AIChE Annual Conference, Reno.

Lazarescu, C., Watanabe, K., and Avramidis, S. (2010). Density and moisture profile evolution during timber drying by CT scanning measurements. Dry. Technol. 28: 460–467.

Lee, C., Dazen, K., Kafle, K., Moore, A., Johnson, D.K., Park, S., and Kim, S.H. (2015). Correlations of apparent cellulose crystallinity determined by XRD, NMR, IR, Raman, and SFG methods. In: Rojas, O.J. (Ed.), *Cellulose chemistry and properties: fibers, nanocelluloses and advanced materials*. Cham: Springer International Publishing, Springer, pp. 115–131.

Lew, C., Clark, J.H., Kraus, G.A., Ackom, E., Gan, J., Patton-Mallory, M., Skog, K.E., Dale, V.H., Kelley, S.S., Wegner, T., et al. (2012). *Integrated forest biorefineries: challenges and opportunities*. *Green Chemistry Series*. Royal Society of Chemistry.

Mast, S.W., Donaldson, L.A., Torr, K., Phillips, L., Flint, H., West, M., Strabala, T.J., and Wagner, A. (2009). Exploring the ultrastructural localization and biosynthesis of β-(1,4)-galactan in Pinus radiata compression wood. Plant Physiol. 150: 573–583.

Mattsson, T., Azhar, S., Eriksson, S., Helander, M., Henriksson, G., Jedvert, K., Lawoko, M., Lindström, M., McKee, L., Oinonen, P., et al. (2017). The development of a wood-based materials-biorefinery. BioResources 12: 9152–9182.

Morohoshi, N. and Sakakibara, A. (1971a). The chemical composition of reaction wood. I. Mokuzai Gakkaishi 17: 393–399, (in Japanese).

Morohoshi, N. and Sakakibara, A. (1971b). The chemical composition of reaction wood. II. Mokuzai Gakkaishi 17: 400–404, (in Japanese).

Muzamal, M., Bååth, J.A., Olsson, L., and Rasmuson, A.S. (2016). Contribution of structural modification to enhanced enzymatic hydrolysis and 3-D structural analysis of steam-exploded wood using X-ray tomography. BioResources 11: 8509–8521.

Nanayakkara, B., Manley-Harris, M., Suckling, I.D., and Donaldson, L.A. (2009). Quantitative chemical indicators to assess the gradation of compression wood. Holzforschung 63: 431–439.

Park, S., Baker, J.O., Himmel, M.E., Parilla, P.A., Johnson, D.K. (2010). Cellulose crystallinity index: measurement techniques and their impact on interpreting cellulase performance. Biotechnol. Biofuels 3: 10.

Procter, A., Yean, W., and Goring, D. (1967). The topochemistry of delignification in kraft and sulphite pulping of spruce wood. Pulp Paper Mag. Can. 68: T445–T460.

Saka, S., Thomas, R., Gratzl, J., and Abson, D. (1982). Topochemistry of delignification in Douglas-fir wood with soda, soda-anthraquinone and kraft pulping as determined by SEM-EDXA. Wood Sci. Technol. 16: 139–153.

Singh, R., Shukla, A., Tiwari, S., and Srivastava, M. (2014). A review on delignification of lignocellulosic biomass for enhancement of ethanol production potential. Renew. Sustain. Energy Rev. 32: 713–728.

Skaar, C. (1988). Moisture movement in the wood cell-wall. In: Skaar, C. (Ed.), *Wood-water relations*. Springer Series in Wood Science. Springer-Verlag, Berlin/Heidelberg, pp. 177–199.

Taiwo, O.O., Finegan, D.P., Paz-Garcia, J.M., Eastwood, D.S., Bodey, A.J., Rau, C., Hall, S.A., Brett, D.J.L., Lee, P.D., and Shearing, P.R. (2017). Investigating the evolving microstructure of lithium metal electrodes in 3D using X-ray computed tomography. Phys. Chem. Chem. Phys. 19: 22111–22120.

Teeäär, R., Serimaa, R., and Paakkarl, T. (1987). Crystallinity of cellulose, as determined by CP/MAS NMR and XRD methods. Polym. Bull. 17: 231–237.

Theander, O. and Westerlund, E.A. (1986). Studies on dietary fiber. 3. Improved procedures for analysis of dietary fiber. J. Agric. Food Chem. 34: 330–336.

Timell, T.E. (1986). Chemical properties of compression wood. In: *Compression wood in gymnosperms*, Vol. 1. Berlin: Springer-Verlag, pp. 289–408.

Trtik, P., Dual, J., Keunecke, D., Mannes, D., Niemz, P., Stähli, P., Kaestner, A., Groso, A., and Stampanoni, M. (2007). 3D imaging of microstructure of spruce wood. J. Struct. Biol. 159: 46–55.

Van den Bulcke, J., Masschaele, B., Dierick, M., Van Acker, J., Stevens, M., and Van Hoorebeke, L. (2008). Three-dimensional imaging

and analysis of infested coated wood with X-ray submicron CT. Int. Biodeterior. Biodegrad. 61: 278–286.

Van den Bulcke, J., Boone, M., Van Acker, J., Stevens, M., and Van Hoorebeke, L. (2009). X-ray tomography as a tool for detailed anatomical analysis. Ann. For. Sci. 66: 1–12.

Van den Bulcke, J., Biziks, V., Andersons, B., Mahnert, K.C., Militz, H., Van Loo, D., Dierick, M., Masschaele, B., Boone, M.N., Brabant, L., et al. (2013). Potential of X-ray computed tomography for 3D anatomical analysis and microdensitometrical assessment in wood research with focus on wood modification. Int. Wood Prod. J. 4: 183–190.

Wagih, A., Maimí, P., Blanco, N., García-Rodríguez, S.M., Guillamet, G., Issac, R.P., Turon, A., and Costa, J. (2019). Improving damage resistance and load capacity of thin-ply laminates using ply clustering and small mismatch angles. Compos. Part A Appl. Sci. Manuf. 117: 76–91.

Walker, J.C.F. (2006). Pulp and paper manufacture (lignin cleavage reactions). In: Walker, J.C.F. (Ed.), *Primary wood processing – principles and practice*. Springer Science & Business Media, Dordrecht, The Netherlands, pp. 504–515.

Walther, T. and Thoemen, H. (2009). Synchrotron X-ray microtomography and 3D image analysis of medium density fiberboard (MDF). Holzforschung 63: 581–587.

Wardrop, A. and Davies, G. (1961). Morphological factors relating to the penetration of liquids into wood. Holzforschung 15: 129–141.

Wardrop, A. (1963). Morphological factors involved in the pulping and beating wood fibres. Sven. Papperstidning 66: 231–247.

Webb, S. (Ed.) (1990). *From the watching of shadows: the origins of radiological tomography*. CRC Press, Bristol, UK, pp. 165–191.

Wernersson, E.L.G., Boone, M.N., Van den Bulcke, J., Van Hoorebeke, L., and Luengo Hendriks, C.L. (2013). Postprocessing method for reducing phase effects in reconstructed microcomputed-tomography data. J. Opt. Soc. Am. A 30: 455–461.

Whiting, P. and Goring, D.A.I. (1981). The topochemistry of delignification shown by pulping middle lamella and secondary wall tissue from black spruce wood. J. Wood Chem. Technol. 1: 111–122.

Whiting, P. and Goring, D.A.I. (1982). Relative reactivities of middle lamellae and secondary wall lignin of black spruce wood. Holzforschung 36: 303–306.

Wigell, A., Brelid, H., and Theliander, H. (2007). Degradation/dissolution of softwood hemicellulose during alkaline cooking at different temperatures and alkali concentrations. Nord. Pulp Pap Res. J. 22: 488–494.

Wojtasz-Mucha, J., Mattsson, C., Hasani, M., and Theliander, H. (2019). Pretreatment and cooking of forest residues. BioResources 14: 9454–9471.

Wood, J., Ahlgren, P., and Goring, D. (1972). Topochemistry in the chlorite delignification of spruce wood topochemistry in the chlorite delignification of spruce wood. Svensk Papperstidning 75: 15–19.

Yoshinaga, A., Ohno, S., and Fujita, M. (2014). Delignification of cell walls of Chamaecyparis obtusa during alkaline nitrobenzene oxidation. J. Wood Sci. 50: 287–294.

Zhao, Ch., Huang, J., Yang, L., Yue, F., and Lu, F. (2019). Revealing structural differences between alkaline and kraft lignins by HSQC NMR. Eng. Chem. Res. 58: 5707–5714.

Supplementary Material: The online version of this article offers supplementary material (https://doi.org/10.1515/hf-2020-0113).